Biomaterials 33 (2012) 7665–7675

Contents lists available at SciVerse ScienceDirect

Biomaterials

journal homepage: www.elsevier.com/locate/biomaterials

Self-assembling nanoparticles for intra-articular delivery of anti-inflammatory proteins

Rachel E. Whitmire [a], D. Scott Wilson [b], Ankur Singh [a], Marc E. Levenston [c], Niren Murthy [d], Andrés J. García [a,*]

[a] George W. Woodruff School of Mechanical Engineering, Georgia Institute of Technology, USA
[b] School of Chemical Engineering, Georgia Institute of Technology, USA
[c] Department of Mechanical Engineering, Stanford University, USA
[d] Department of Bioengineering, University of California, Berkeley, USA

ARTICLE INFO

Article history:
Received 15 June 2012
Accepted 30 June 2012
Available online 17 July 2012

Keywords:
IL-1Ra
Nanoparticles
Block copolymer
RAFT polymerization
Osteoarthritis
Drug delivery

ABSTRACT

Intra-articular delivery of therapeutics to modulate osteoarthritis (OA) is challenging. Delivery of interleukin-1 receptor antagonist (IL-1Ra), the natural protein inhibitor of IL-1, to modulate IL-1-based inflammation through gene therapy or bolus protein injections has emerged as a promising therapy for OA. However, these approaches suffer from rapid clearance and reduced potency over time. Nano/microparticles represent a promising strategy for overcoming the shortcomings of intra-articular drug delivery. However, these delivery vehicles are limited for delivery of protein therapeutics due to their hydrophobic character, low drug loading efficiency, and harsh chemical conditions during particle processing. We designed a new block copolymer that assembles into submicron-scale particles and provides for covalently tethering proteins to the particle surface for controlled intra-articular protein delivery. This block copolymer self-assembles into 300 nm-diameter particles with a protein tethering moiety for surface covalent conjugation of IL-1Ra protein. This copolymer particle system efficiently bound IL-1Ra and maintained protein bioactivity *in vitro*. Furthermore, particle-tethered IL-1Ra bound specifically to target synoviocyte cells via surface IL-1 receptors. Importantly, IL-1Ra nanoparticles inhibited IL-1-mediated signaling to equivalent levels as soluble IL-1Ra. Finally, the ability of nanoparticles to retain IL-1Ra in the rat stifle joint was evaluated by *in vivo* imaging over 14 days. IL-1Ra-tethered nanoparticles significantly increased the retention time of IL-1Ra in the rat stifle joint over 14 days with enhanced IL-1Ra half-life (3.01 days) compared to that of soluble IL-1Ra (0.96 days) and without inducing degenerative changes in cartilage structure or composition.

1. Introduction

Osteoarthritis (OA) is a highly prevalent and debilitating condition with staggering socioeconomic costs. Arthritis and related conditions are estimated to cost the U.S. economy $128 billion per year in medical care and indirect expenses [1]. OA is the most common form of arthritis, affecting nearly 27 million Americans [2]. Epidemiological studies indicate that some evidence of OA can be found in 60% of the population over age 35, with radiographic evidence of cartilage thinning in more than 50% of adults over age 65 [3].

OA is characterized by progressive degradation of articular cartilage, typically in load-bearing areas of one or more joints. Current pharmacological treatments for OA mostly focus on pain relief [4]. OA symptoms can be alleviated by oral analgesics, systemic non-steroidal anti-inflammatory drugs, and intra-articular injection of glucocorticosteroids [3–6]. Inflammatory mediators such as cytokines interleukin-1 (IL-1), IL-6, IL-8, IL-13, reactive oxygen species (ROS), and proteases including multiple matrix metalloproteinases and ADAMTS enzymes play central roles in the progression of OA [7–10]. Consequently, anti-inflammatory drugs are being explored for treating arthritis through intra-articular injections. For instance, IL-1Ra has been delivered using gene therapy approaches or bolus protein injections [11–17]. However, these anti-inflammatory therapies have not been effective and are limited by currently available drug delivery materials. In particular, a major challenge is rapid clearance of the injected agent from the joint, which significantly decreases the therapeutic effect and reduces the benefits of local administration.

* Corresponding author. Fax: +1 404 385 1397.
E-mail address: andres.garcia@me.gatech.edu (A.J. García).

0142-9612/$ – see front matter © 2012 Elsevier Ltd. All rights reserved.
http://dx.doi.org/10.1016/j.biomaterials.2012.06.101

Effective delivery of therapeutic proteins is a major goal of current biomaterial-based strategies. Current delivery strategies can efficiently encapsulate hydrophobic drugs without losing their effectiveness or bioactivity [18–20]. However, these systems have critical disadvantages for protein delivery. The hydrophobicity of many drug-delivering polymers (e.g., PLGA) severely reduces or destroys the bioactivity of encapsulated proteins [21–23]. Liposomes provide a hydrophilic encapsulation environment, but are limited by their instability *in vivo* [24,25]. Other strategies for extending a protein's half-life include PEGylating native proteins for systemic injection [26–28], creating drug depots [29,30], and encapsulating proteins in polymer particles for local protein delivery [31–33]. Although these technologies have increased protein half-life, their overall efficacy is limited by the associated loss of protein bioactivity and low protein loading capacity.

The goal of this study was to (1) develop a new block copolymer that assembles into nanoparticles that efficiently tether IL-1Ra protein onto their surface, (2) characterize this system for biological activity and target specificity, and (3) evaluate intra-articular retention of therapeutic protein in the rat stifle joint space.

2. Materials and methods

All reagents were obtained from Sigma–Aldrich (St. Louis, MO, USA) and used as is, unless otherwise specified.

2.1. Synthesis of the modified μ-RAFT agent

2.1.1. Synthesis of the intermediate 17-hydroxy-3,6,9,12,15-pentaoxaheptadecyl 2-((phenylcarbonothioyl)thio)acetate–(intermediate-1)

N,N′-dicyclohexylcarbodiimide (DCC) (619.0 mg, 3.0 mmol) was dissolved in 5 mL dichloromethane (DCM) and added drop-wise to a stirred solution of (benzothioylsulfanyl)acetic acid (500 mg, 2.36 mmol), hexaethylene glycol (1.41 g, 5.0 mmol), and a catalytic amount of 4-dimethylaminopyridine (DMAP) in 50 mL DCM at 0 °C. After adding DCC, the solution was allowed to reach room temperature. After 2 additional hours of stirring, the solutions were filtered, and the organic solution was concentrated via rotary evaporation, resuspended in ethyl acetate, and finally evaporated onto silica gel. The desired product was isolated by flash silica gel chromatography on silica gel, using a mixture of ethyl acetate and hexanes (6:4).

2.1.2. Synthesis of the final modified μ-RAFT agent 1-(4-nitrophenoxy)-1-oxo-2,5,8,11,14,17-hexaoxanonadecan-19-yl 2-((phenylcarbonothioyl)thio)acetate

A solution of 4-nitrophenyl chloroformate (201 mg, 1.0 mmol) in 1 mL of DCM was added drop-wise to a stirred solution of intermediate-1 (476 mg) and pyridine (95 mg, 1.5 mmol) maintained at 0 °C. After 1 h of stirring, the solutions were filtered, and the organic solution was concentrated via rotary evaporation, resuspended in ethyl acetate, and finally evaporated onto silica gel. The desired product was isolated via flash silica gel chromatography on silica gel using a mixture of ethyl acetate and hexanes (4:6).

2.2. Tetraethylene glycol methacrylate (TEGM) monomer synthesis

Tetraethylene glycol (5.0 g, 25.7 mmol) (#110175, Aldrich), and pyridine (2.0 g, 25.3 mmol) (#PX20202-5, EMD, Gibbstown, NJ, USA) were added to anhydrous dichloromethane (DCM) (100 mL) in a 250 mL flask and stirred for 30 min at 0 °C. Methacryloyl chloride (2.6 g, 25 mmol) (#64120, Sigma–Aldrich) was added drop-wise to the stirred solution. The reaction was allowed to stir at 0 °C for 2 h, and then at room temperature for an additional 2 h. The product was then concentrated via rotary evaporation, resuspended in ethyl acetate, and evaporated onto silica gel. The monomethacrylate product was separated from the di-methacrylate byproduct and any remaining starting materials via flash silica gel chromatography on silica gel, using a mixture of ethyl acetate and hexanes (7:3).

2.3. Block copolymer synthesis

The block copolymer was synthesized by RAFT polymerization, in which the nitrophenyl-functionalized μ-RAFT initiator was used to initiate the polymerization of the hydrophilic monomer TEGM and then the hydrophobic monomer cyclohexyl methacrylate. The polymers were characterized using GPC and NMR (Fig. 1).

2.3.1. Hydrophilic block synthesis

TEGM (0.9 g, 3.43 mmol), μ-RAFT agent (22.0 mg, 0.034 mmol), and AIBN (0.5 mg, 0.003 mmol) were combined in DMF (1.5 mL). The reaction flask was degassed by five freeze–pump–thaw cycles, and was then immersed in an oil bath and stirred at 65 °C. After 20 h, the reaction was terminated by flash freezing in liquid nitrogen. The reaction product was added to DCM (5 mL) and then was precipitated from methanol (25 mL). The supernatant was decanted and the precipitated polymer was subjected to three more rounds of resuspension (DCM) and precipitation (MeOH) before being concentrated under reduced pressure. The purified polymer was analyzed for weight by gel permeation chromatography (THF) and the structure and purity of the resulting polymer were verified by ^{1}H NMR.

2.3.2. Hydrophobic block synthesis

Polymerized TEGM (0.5 g, 1.90 mmol), cyclohexyl methacrylate (213.65 mg, 1.27 mmol) (Tokyo Chemical Industry Co, Ltd., Tokyo, Japan) and AIBN (0.25 mg, 0.0015 mmol) were combined in DMF (1.5 mL). The reaction flask was degassed by five freeze–pump–thaw cycles and was then immersed in an oil bath and stirred at 65 °C. After 20 h, the reaction was terminated by flash freezing in liquid nitrogen. The reaction product was added to DCM (5 mL) and was precipitated using methanol (25 mL). The supernatant was decanted and the precipitated polymer was subjected to three more rounds of resuspension (DCM) and precipitation (MeOH) before being concentrated under reduced pressure. The purified polymer was analyzed for molecular weight by gel permeation chromatography (THF) and the structure and purity were verified by ^{1}H NMR.

2.4. Polymer characterization

2.4.1. ^{1}H NMR and ^{13}C NMR analysis

Samples of the modified components (μ-RAFT, TEGM) and the 2 steps in the copolymer synthesis were dried under vacuum to remove excess solvent. The samples were resuspended in $CDCl_3$ for NMR analysis. All analyses were run on a 400 MHz low-field NMR (Oxford Instruments, Oxfordshire, England).

2.5. Particle formation and protein tethering

Copolymer was dissolved in THF at a concentration of 40 mg/mL. The copolymer requires at least 48 h to fully resolubilize after resuspending it in solvent. To make particles, 50 mL of 0.01 M phosphate-buffered saline (PBS) was added to a 150 mL beaker and was set on a stir plate at 400 rpm. The polymer (20 mg) was dissolved in 2.5 mL THF/DMF (9:1) and was added to the aqueous phase at 20 mL/h using a syringe pump (10 mL syringe, 18 gauge needle). Once the polymer was added, the solution was transferred to a 250 mL round-bottom flask and the solvent was evaporated under reduced pressure for 30 min to remove THF. The particle solution was concentrated by centrifugation using 100 kDa centrifugal filters Amicon Ultra-4 Centrifugal Filters with Ultracel-100 kDa membranes (Millipore, Billerica, MA USA) for 3 min at 2750 rpm, and was then sonicated for 30 s to resuspend any clumped particles.

IL-1Ra or bovine serum albumin (BSA) protein was added to the particle solution and the pH was raised to 8.0 using 0.01 M NaOH. The particle/protein solution was allowed to react overnight at 4 °C. Ten mg/mL glycine in PBS was added to quench any remaining reactive groups and was allowed to react for 30 min at 4 °C. The particle solutions were transferred to 10 kDa dialysis cassettes and were dialyzed overnight against PBS with at least 3 buffer changes. The particles were transferred to sterile microcentrifuge tubes and stored at 4 °C until further use.

2.6. Particle size characterization

Particle size was analyzed by dynamic light scattering using a 90 Plus Particle Size Analyzer (Brookhaven Instruments Corporation, Holtsville, NY).

2.7. Fluorescent protein labeling

IL-1Ra or bovine serum albumin was labeled prior to coupling to particles using commercial labeling fluorescent reagents according the manufacturer's instructions. Proteins were labeled with Alexa Fluor 488 to visualize the particles during *in vitro* experiments. Protein (IL-1Ra or BSA) was reacted with Alexa Fluor 488 maleimide (Invitrogen, Carlsbad, CA) according to the manufacturer's instructions. There are 3 free solvent-accessible cysteines on IL-1Ra that can be fluorescently tagged [34]. The resulting fluorescently tagged proteins are denoted AF-488-IL-1Ra and AF-488-BSA. For the confocal study, AF-594 was used to fluorescently label IL-1Ra (AF-594-IL-1Ra). Labeled proteins were stored in PBS at 4 °C until use.

For *in vivo* imaging experiments, IL-1Ra was labeled with near-IR dye. IL-1Ra was reacted with Alexa Fluor 750 maleimide (Invitrogen, Carlsbad, CA, USA) or DyLight 650 maleimide (#62295, Pierce, Rockford, IL, USA). By fluorescently labeling the cysteines on IL-1Ra, we avoided using the more prevalent amines, thereby allowing the protein to be fluorescently labeled before tethering it to particles, as well as reducing the chance of altering the protein's bioactivity [34]. AF-650-labeled IL-1Ra-tethered particles were used to evaluate particle targeting and localization within the intra-articular joint space.

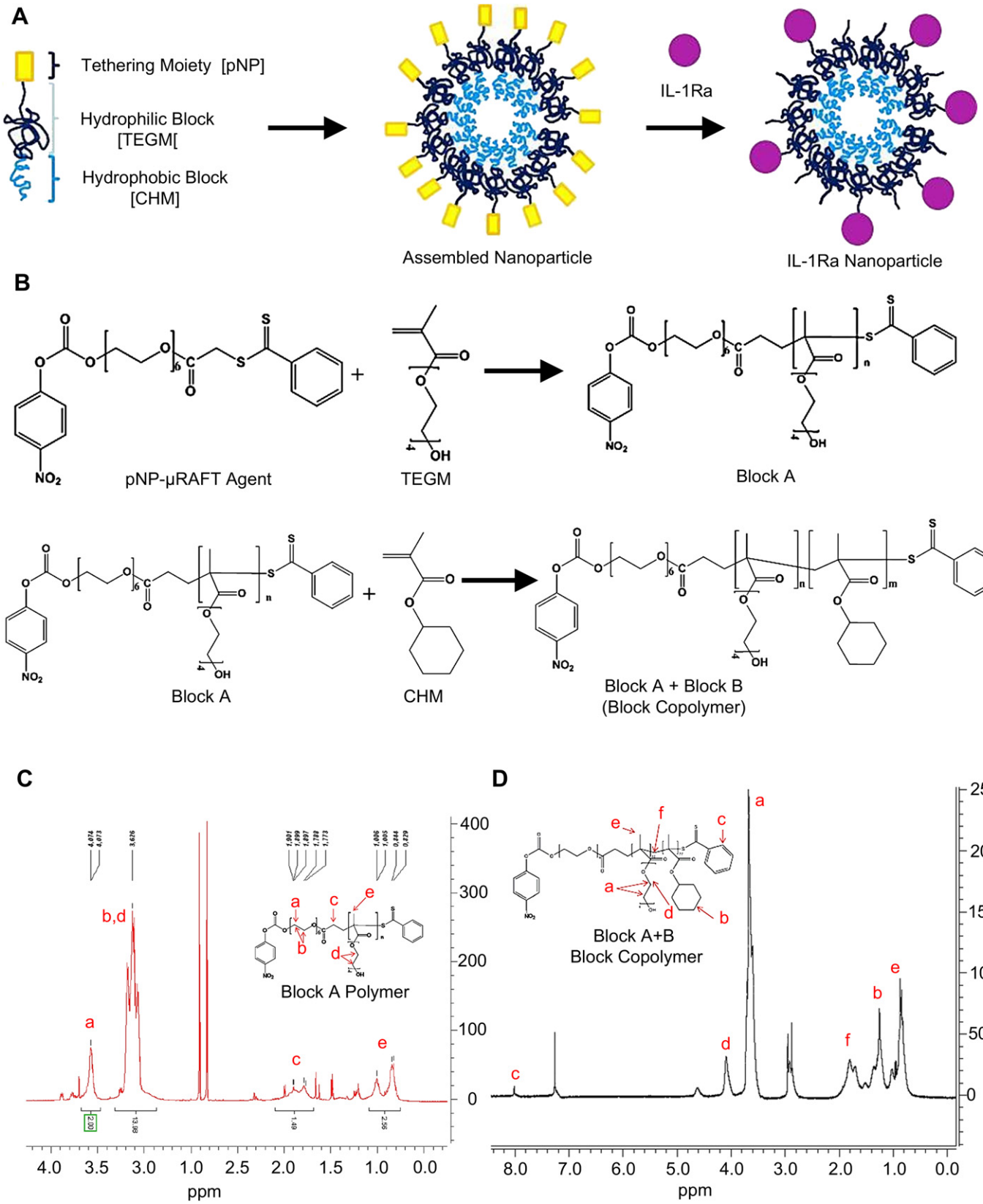

Fig. 1. Protein tethering block copolymer. A) Schematic of self-assembly of the nanoparticles and protein conjugation. **B)** A modified commercial RAFT agent (μ-RAFT) was used for polymerization. Tetraethylene glycol methacrylate and μ-RAFT were mixed and polymerization was initiated using AIBN. Monomeric cyclohexyl methacrylate was added to the product of the first reaction (block A) and polymerization was re-initiated to form the copolymer (block A + B). **C)** The synthesis of the copolymer is confirmed by ^{1}H NMR. The block A polymer synthesis was confirmed by ^{1}H NMR. Peaks were observed at 3.7 ppm (14H, 13.98) (c, f), 4.2 ppm (2H, 2.0) (b, e), 1.9 ppm (2H, 1.49) (g), and 0.9–1.1 ppm (3H, 2.56) (a, h). **D)** The synthesis of the block A + B (copolymer) was confirmed by ^{1}H NMR. Peaks were observed at 3.6 ppm (m*14H) (a), 4.1 ppm (m*2H) (d), 1.3 ppm (n*10H) (b), 0.9 ppm (m*3H, n*3H) (e), 1.9 ppm (6H) (f), and 7.0 ppm (9H) (c). m = number of TEGM monomers; n = number of CHM monomers.

2.8. In vitro characterization

2.8.1. Cytotoxicity assay

RAW 264.7 macrophage cells (TIB-71, ATCC, Manassas, VA) were cultured in Dulbecco's Minimum Essential Media (DMEM) supplemented with 10% fetal bovine serum (FBS) at 37 °C, 5% CO_2. RAW macrophages were seeded on a tissue culture treated plastic surface and allowed to adhere for 4 h. Supernatant was removed and replaced with serum-free DMEM overnight to quiesce the cells. The next morning, 0.5 mL of phenol-red-free DMEM + particles was added at particle concentrations of 0.1, 1, and 10 mg/mL. The cells were incubated with the particles in serum-free media for 6 h before analysis using the MTT (3-(4,5-dimethylthiazol-2-yl)-2,5-diphenyltetrazolium bromide) assay. The MTT assay measures the oxidation of MTT dye by cellular reductase enzymes. It measures cellular metabolic activity and is used as an indirect measure of cell viability and proliferation. MTT substrate (50 μL) was added to each well and was incubated for 2 h at 37 °C. HCl (0.5 mL, 0.1 M) was added to each well to develop the substrate. Each well content was pipetted to mix and then transferred to a 96-well plate for colorimetric detection using a plate reader at 570 nm (HTS 7000 Plus, Perkin Elmer, Waltham, MA, USA).

2.8.2. Synoviocyte binding experiments

The HIG-82 synoviocyte cell line (CRL-1832, ATCC, Manassas, VA, USA) was originally derived from a female rabbit whose synoviocytes were harvested and immortalized [35,36]. Cells were cultured in Ham's F-12 supplemented with 10% heat-denatured FBS at 37 °C, 5% CO_2. Cells were removed from culture using 0.25% trypsin + 0.5 mM EDTA. Cells were counted and plated at 2.1×10^4 cells/cm^2. After 6 h of incubation, the medium was replaced with serum-free medium and the cells cultured overnight. The next day, approximately 3,000 particles (equivalent to 0.1 μg IL-1Ra/mL) IL-1Ra- or BSA-functionalized particles were added to the cells and incubated for 2 h at 37° and 5% CO_2. Some samples were incubated with 50 μg/mL IL-1β for 2 h to block the available IL-1 receptors prior to adding the particles. Cells were analyzed for particle binding by confocal microscopy and flow cytometry.

For confocal microscopy analysis, HIG-82 cells were plated overnight on glass covers with 8-well divisions (Lab-Tek™ Chambered Coverglass, Thermo Scientific, Rochester, NY, USA). The next morning, 30 μL of either AF-594-IL-1Ra-tethered particles or AF-488-BSA-tethered particles (~30,000 particles each) were added to serum-free Ham's F12 media for a total volume of 3.2 mL. Each well received 200 μL of media ± particles and was incubated for 2 h at 37 °C, 5% CO_2. After rinsing with PBS three times to remove unbound particles, cell nuclei were stained with Hoechst for 15 min and samples were imaged using a Nikon TE300 microscope equipped with a C1-Plus LU-4A AOTF Confocal System (particles: IL-1Ra: AF-594/red; BSA: AF488/green; cell nuclei: Hoechst/blue).

For flow cytometry analysis, HIG-82 cells were plated on 12-well plates and serum starved overnight. The next morning, particles (IL-1Ra or BSA) in fresh serum-free Ham's F12 medium were added to each well for 2 h. After washing three times with PBS, the cells were detached from the culture plates using trypsin-EDTA and were resuspended in serum-containing media. The cell suspensions were analyzed on an Accuri C6 Flow Cytometer (BD Accuri Cytometers, Ann Arbor, MI, USA).

2.8.3. Inhibition of IL-1β-induced signaling

NIH 3T3 cells stably transfected with an NF-κB-luciferase reporter construct were a gift from Dr. van de Loo (Radboud University, Nijmegen, Netherlands) [37], and produced luciferase under control of an NF-κB-responsive promoter. NIH 3T3 NF-κB-luc cells were plated in 96-well plates at a density of 1×10^5 cells/mL (100 μL/well) in DMEM with 10% FBS. Cells were allowed to adhere for 6 h before replacing the media with serum-free DMEM + 1 mM sodium pyruvate and incubation overnight. Thereafter, IL-1Ra-tethered particles, BSA-tethered particles, or soluble IL-1Ra was added to each well (1 μg/mL IL-1Ra or equivalent amount of polymer for protein-tethered particles) and was incubated for 1 h. Then, 10 pg IL-1β was added to each well to stimulate NF-κB activation (final concentration of 0.1 ng/mL IL-1β). Cells were incubated with IL-1β for 6 h before washing 3 times with PBS. Cells were then lysed with 20 μL of Passive Lysis Buffer (Promega, Madison, WI) for 20 min on a gentle vortexer. Lysate (20 μL) was added to 100 μL of luciferase substrate in an opaque white 96-well plate. Luminescence was read using a plate reader (HTS 7000 Plus, Perkin Elmer, Waltham, MA).

2.9. Intra-articular delivery and retention in an animal model

2.9.1. Animal model

Male Lewis rats (10–12 week old) received 50 μL of either particles or soluble IL-1Ra protein (5 μg IL-1Ra) via intra-articular injection to the right stifle joint space, while the left stifle received the equivalent volume of saline and served as a contralateral control. Rats were deeply anesthetized with isofluorane. The hair was removed from the hind limb surgical sites and the skin was cleaned with alcohol. Rats were positioned on their back, and the leg was flexed to 90° at the stifle joint. Particles were injected into the intra-articular space by palpating the patellar ligament below the patella and injecting the particle solution through the infrapatellar

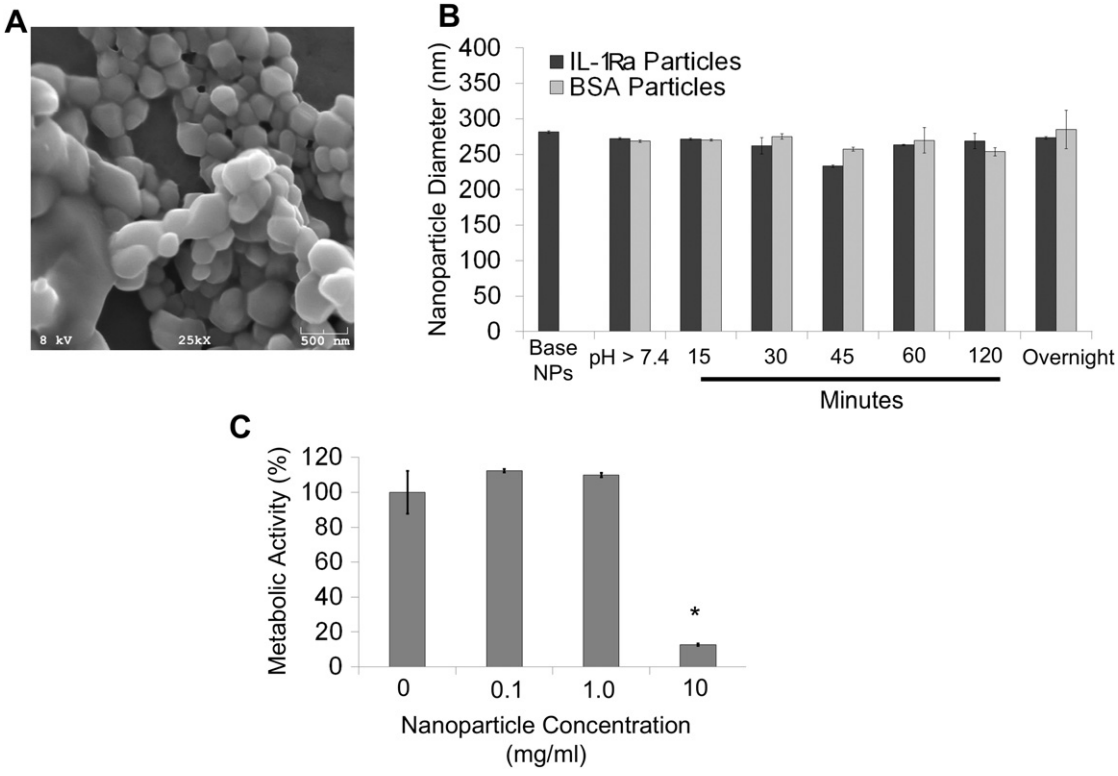

Fig. 2. Block copolymer forms nanoparticles. A) SEM images of nanoparticles. Nanoparticle size was confirmed by scanning electron microscopy. **B)** Dynamic light scattering based sizing of particles. Nanoparticle diameters were measured using a refractive index of 1.33 (water). Nanoparticles were measured after rotary evaporation of solvent (rotovap) referred to as base nanoparticles; after raising the pH to initiate protein tethering (pH > 7.4), and at 15, 30, 45, 60, 120 min, and overnight after adding protein to the particles. **C)** MTT assay for cytotoxicity for cells incubated with nanoparticles.

ligament using a sterile 27-gage 0.5" needle. Rats were fully ambulatory following recovery and all injections were well tolerated. At the end point of the study, rats were euthanized using CO_2 asphyxiation. All procedures were approved by Georgia Tech's Institutional Animal Care and Use Committee.

2.9.2. IVIS imaging to evaluate particle retention

Rats were anesthetized using isofluorane. Animals receiving IR-750-IL-1Ra-tethered particles or soluble IR 750-labeled IL-1Ra were scanned in an IVIS imaging system (700 Series, Caliper Xenogen IVIS Lumina, Caliper Life Sciences, Hopkinton, MA, USA). The excitation and emission detectors were set at 745 nm and 780 nm, respectively. Both hind limbs were scanned to control for background tissue fluorescence. The total photons within a fixed region centered on the stifle were measured and were analyzed with non-linear regression models. The data from each animal were normalized to their individual day 0 values. The normalized data were fitted using a one-phase exponential decay with the characteristic equation of:

$$F = (F_o - NS) \times e^{(-K \times t)} - NS$$

where F is the fluorescence photon counts, F_o is the intersection of the best-fit line with the Y-axis, NS is the non-specific binding value (i.e., the asymptotic y-value), t is time, and K is inversely proportional to the half-life. Data was analyzed using GraphPad Prism 5.0 (GraphPad Software, La Jolla, CA, USA).

2.9.3. Immunostaining to evaluate particle retention

To determine retention of IL-1Ra nanoparticles in knee joints, animals were injected with Dylight-IR-650-IL-1Ra-tethered particles or soluble Dylight-IR-650-IL-1Ra protein. After 3 days, animals were sacrificed and stifle joints were harvested, fixed in 10% neutral buffered formalin for 48 h and decalcified using Cal-Ex II for 14 days. Samples were cut down the longitudinal axis, creating two cylindrical halves, and each half was sectioned using a cryosectioner (10 μm thick sections). Sections were counterstained with DAPI and imaged using confocal microscopy.

2.9.4. EPIC-μCT

μCT has been established as an effective, non-destructive technique for imaging cartilage [38–40]. EPIC-μCT employs interactions between a charged contrast agent

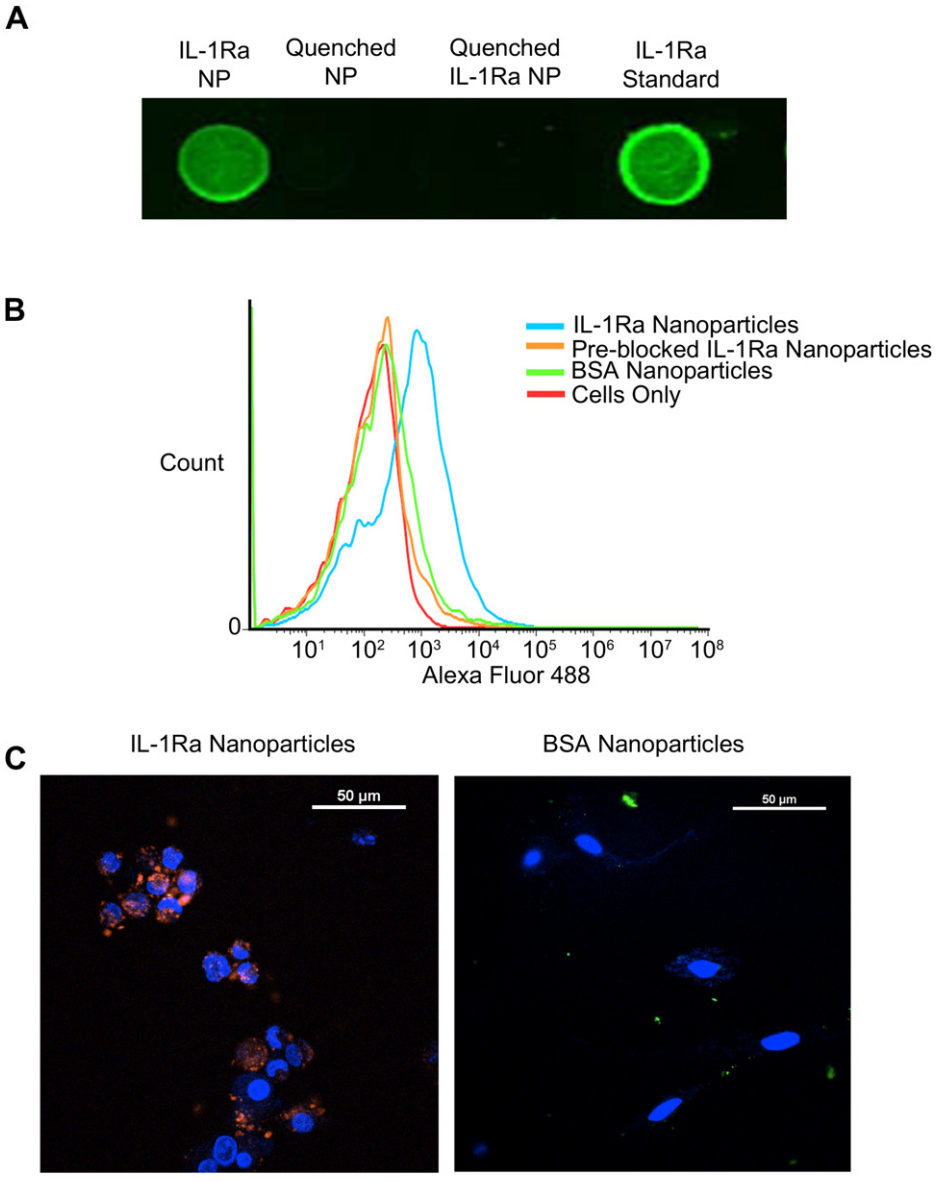

Fig. 3. Protein tethering and target specificity for IL-1Ra nanoparticles. A) Dot Blot: IL-1Ra-tethered particles, glycine-tethered particles, or soluble IL-1Ra were dried on nitrocellulose membranes and were probed with anti-IL-1Ra antibodies. Blots were imaged using near infrared (800 nm) secondary antibodies and an infrared imager. **B)** IL-1Ra-tethered nanoparticles bind to synoviocytes in an IL-1R-dependent manner. A synoviocyte cell line (HIG-82) was incubated with fluorescently tagged IL-1Ra-tethered particles or fluorescently tagged BSA-tethered particles, with or without an IL-1β pre-blocking step and assayed using flow cytometry. Synoviocytes + IL-1Ra-Particles (44.0% cells with bound nanoparticles), Blue; synoviocytes + BSA-Particles (2.7%), green; synoviocytes + Pre-Block + IL-1Ra-Particles, (2.8%), Orange; synoviocytes only (0.1%), red. **C)** Confocal microscopy images showing that IL-1Ra-tethered particles are bound by synoviocytes: Confocal microscopy Analysis. Particles were incubated with a synoviocyte cell line (HIG-82) for 2 h. Samples were rinsed three times with PBS before imaging. IL-1Ra-tethered particles, red; BSA-tethered particles, green; nuclei, blue. Ten fields from 4 samples of each group were analyzed. (For interpretation of the references to color in this figure legend, the reader is referred to the web version of this article.)

and the sulfated glycosaminoglycans (sGAGs) in the cartilage to render the tissue radiopaque and allow quantification of cartilage morphology and sGAG distribution. Negatively charged agents are excluded from healthy cartilage tissue due to the presence of negatively charged sGAG, and degenerative cartilage exhibits increased contrast agent concentration due to reduced sGAG concentration. Rat stifle joints were evaluated by μCT for cartilage integrity and thickness. Briefly, each explanted rat joint was immersed in 2 mL of 30% Hexabrix 320 (Mallinckrodt, Hazelwood, MO, USA) in PBS at 37 °C for 30 min. The stifle joint was patted dry on a paper towel to remove excess Hexabrix and then was placed in a 16 mm-diameter CT tube and was inserted into the CT machine (μCT 40, Scanco Medical, Bassersdorf, Switzerland). The attenuation was thresholded to isolate the cartilage layer, and trabecular thickness and volume algorithms were used to quantify the morphology of the thresholded cartilage. The following settings were used: 45 kVp, 176 μA, 200 ms integration time, a 1024 × 1024 pixel matrix, and a 16 μm voxel size. Each joint scan was first reformatted to vertical slices, contoured by hand and then evaluated for cartilage thickness and attenuation. Reconstructions were done using sigma = 1, support = 1, lower = 75, upper = 220, and unit = 6.

2.9.5. Histology

Rat distal femora were fixed in 10% neutral buffered formalin for 48 h and decalcified using Cal-Ex II for 14 days. Femora were cut down the longitudinal axis, creating two cylindrical halves. All samples were processed and embedded in glycol methacrylate (GMA) following the manufacturer's protocol (Polysciences, Warrington, PA, USA). After GMA embedding, 2 μm-thick sections through the entire explant thickness were removed using a tungsten-carbide blade on a rotary microtome. Sections were stained with hematoxylin and eosin or with an aqueous solution of 0.1% safranin-O with 0.2% Fast Green as a counterstain to detect sGAGs.

2.10. Statistics

Non-linear regression analysis was performed using GraphPad Prism. Analysis of variance (ANOVA) statistical analyses were performed using SYSTAT 11 software with Tukey's test for pairwise comparisons. A p-value of 0.05 was considered significant.

3. Results

We sought to engineer an amphiphilic block copolymer with a stable protein tethering moiety that assembles into submicron-scale particles and allows for protein tethering to the particle surface.

3.1. Block copolymer synthesis

Fig. 1A shows a schematic for the proposed block copolymer. We used a modified RAFT compound, referred herein as the μ-RAFT agent, as the foundation for our block copolymer. RAFT agents have been used to form a large library of low-polydispersity living polymers, including block copolymers [41]. We modified a commercial μ-RAFT agent with a paranitrophenol (pNP) group to allow the polymer's subsequent functionalization with peptides (Fig. 1A). The modification of the μ-RAFT agent was confirmed by ^{1}H NMR, ^{13}C NMR, and FTIR. The μ-RAFT agent was used to polymerize the tetraethylene glycol methacrylate (TEGM) monomer to create the hydrophilic block A polymer (Fig. 1B). Polymerization was re-initiated in the presence of the hydrophobic monomer cyclohexyl methacrylate to add the hydrophobic block B to the existing block A polymer in order to create an amphiphilic block copolymer. We confirmed this polymerization by ^{1}H NMR for block A (Fig. 1C) and block A + B (Fig. 1D). The molecular weight of block A was 2700 Da and block B was 13,000 Da, for a total MW of 15,700 Da estimated by gel permeation chromatography.

3.2. Particle fabrication and characterization

The polymer spontaneously assembled into particles with an average diameter of 270 ± 5 nm when dropped into stirred PBS, as indicated by scanning electron microscopy (Fig. 2A) and dynamic light scattering (Fig. 2B). Furthermore, the nanoparticles retained their size upon overnight incubation with protein at slightly basic conditions (pH > 7.4) (Fig. 2B).

3.3. Particle cytotoxicity

RAW macrophages were incubated with polymer particles (no tethered protein) at a range of concentrations (0, 0.1, 1.0, 10 mg/mL) to determine the cytotoxicity of these particles. The metabolic

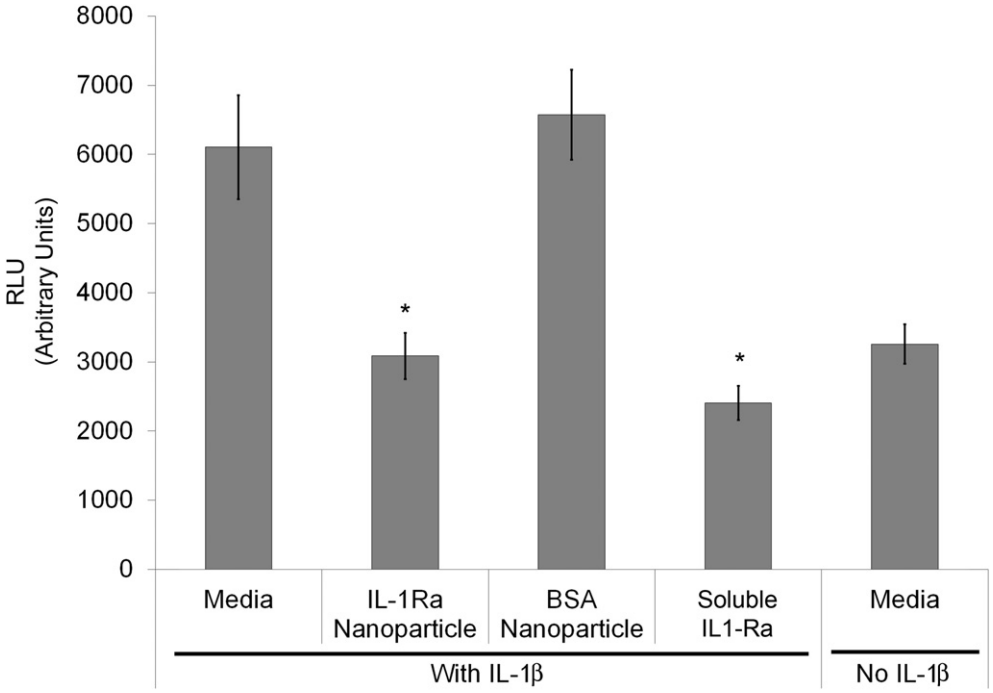

Fig. 4. IL-1Ra-tethered particles inhibit IL-1β-induced NF-κB activation. NIH 3T3 fibroblasts with an NF-κB-responsive luciferase reporter construct were pre-incubated for 1 h with 1 μg/mL IL-1Ra-tethered particles, BSA-tethered particles, or soluble IL-1Ra before stimulating with 0.1 ng/mL IL-1β for 6 h. Both IL-1Ra particles and soluble IL-1Ra inhibited NF-κB activation to comparable levels with unstimulated controls ($n = 3$), $^{*}p < 0.004$.

activity of the cells was assayed by the MTT assay and used as a measure of cytotoxicity. The cells maintained their metabolic activity at doses up to 1 mg/mL. However, metabolic activity was significantly reduced at the 10 mg/mL dose compared to untreated cultures (Fig. 2C), suggesting cytotoxicity at these high concentration.

3.4. Tethering protein to the particle surface

We next evaluated protein tethering onto the particle surface. The polymer design incorporates a 4-nitrophenol group (pNP), which is displaced by primary amines to form a peptide bond at slightly basic pH. To demonstrate that protein is tethered to the nanoparticles, we made particles as described above, raised the pH using sterile NaOH and added 1 mg of IL-1Ra. The nanoparticles were lyophilized and analyzed for protein attachment by dot blot. Fig. 3A shows that the nanoparticles presented strong IL-1Ra antibody staining, demonstrating that IL-1Ra was successfully tethered to the particles. Dot blot analysis with an antibody against IL-1Ra showed high tethering efficiency with 250 ng IL-1Ra/100 μg particles, corresponding to 6–8 IL-1Ra molecules/nanoparticle.

3.5. Bioactivity and target specificity of IL-1Ra-particles

The bioactivity and target specificity of IL-1Ra-tethered nanoparticles were evaluated by assessing the ability of IL-1Ra-tethered particles to bind to HIG-82 synoviocytes. Synoviocytes were incubated with IL-1Ra- or BSA-tethered nanoparticles and analyzed by flow cytometry. Synoviocytes incubated with IL-1Ra-tethered particles exhibited higher fluorescence intensity compared to untreated cells or cells incubated with control BSA-tethered particles (Fig. 3B), demonstrating binding of IL-1Ra-particles to cells. Furthermore, cells that were incubated with high levels of IL-1β to saturate IL-1 receptors prior to particle exposure showed reduced binding of IL-1Ra-tethered particles compared to control levels, indicating that IL-1Ra binds to IL-1 receptors. We also verified particle binding to cells of interest by confocal microscopy. Synoviocytes were incubated with IL-1Ra-particles or BSA-particles and imaged by confocal microscopy. The samples incubated with IL-1Ra-particles had a significantly higher co-localization of particles (green) and cell nuclei (blue) than the BSA-particles samples (Fig. 3C).

3.6. Effect of IL-1Ra-particles on IL-1β-induced signaling

To test whether IL-1Ra-tethered particles could inhibit IL-1β-mediated signaling, we used an IL-1-responsive cell line stably expressing a luciferase construct driven by an NF-κB-responsive promoter. Binding of IL-1β to cellular receptors activates NF-κB as part of its signaling pathway [42]. We measured the effectiveness of IL-1Ra-tethered particles towards blocking IL-1β-induced activation of NF-κB by pre-incubating these cells for 1 h with soluble

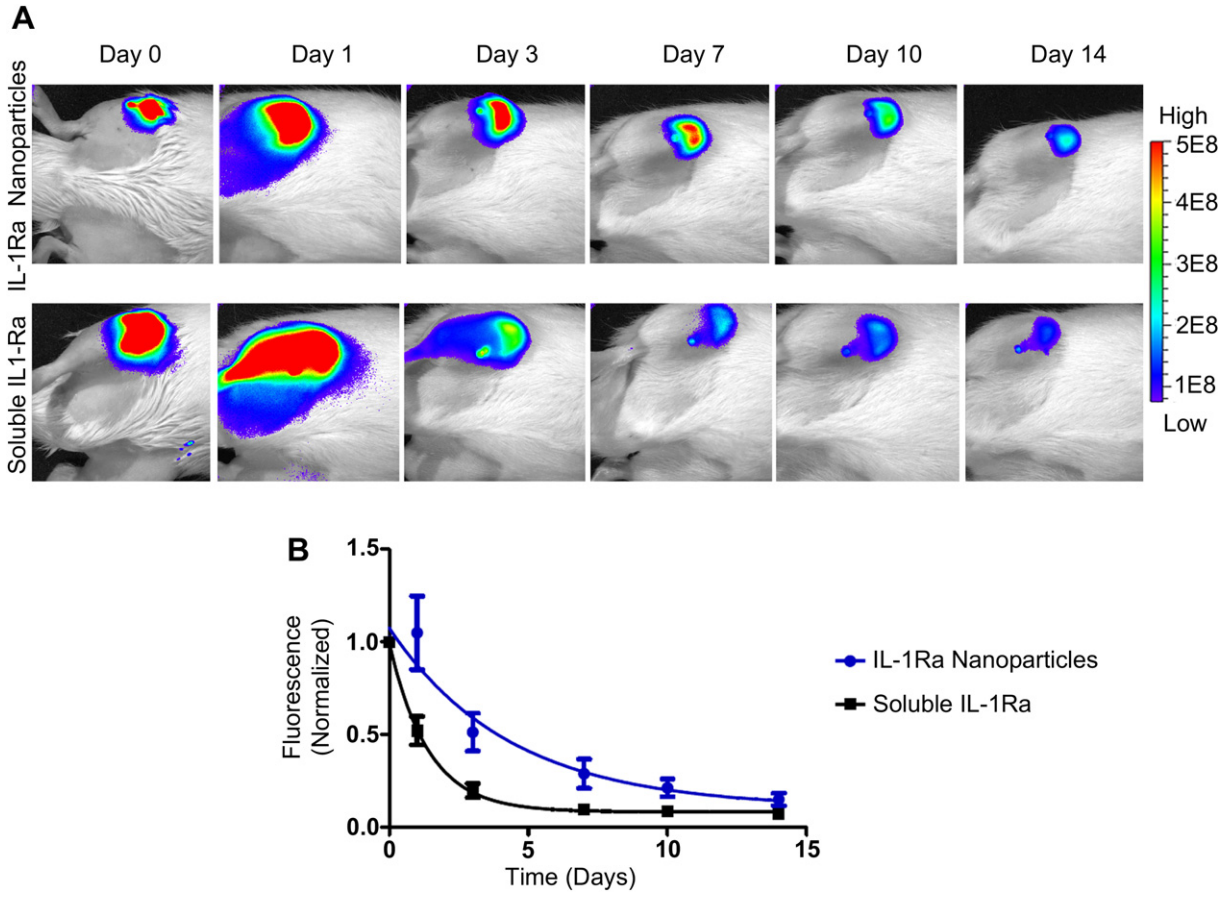

Fig. 5. IL-1Ra-tethered particles are retained longer than soluble IL-1Ra in the intra-articular joint space. A) Representative images of labeled IL-1Ra. IL-1Ra was tagged with a near-IR dye (AF750-maleimide) prior to tethering IL-1Ra to particles. IL-1Ra-tethered particles or soluble IL-1Ra was injected into the right stifle joint of 8–10 wk old rats. Left stifle joints were injected with saline at the same time. Total IR photon counts (relative fluorescence units) within a fixed area centered over the rat's joint were measured by IVIS imaging over 14 days. **B)** IL-1Ra-particles show sustained signal compared to soluble IL-1Ra. Infrared (IR) photon counts were measured in each rat over 14 days by an IVIS imaging system. All data were normalized by individual rat to its day 0 photon count. The photon's signal decay was fit using a one-phase exponential decay model. Half-life: 3.01 ± 0.09 days for IL-1Ra-particles ($n = 6$) vs. 0.96 ± 0.08 days for soluble IL-1Ra ($n = 5$).

IL-1Ra, IL-1Ra-tethered particles, or BSA-tethered particles. When stimulated with IL-1β, only IL-1Ra-particles and soluble IL-1Ra (positive control) effectively inhibited NF-κB activation to baseline levels (Fig. 4). BSA-particles showed no inhibitory effects on NF-κB activity. Remarkably, the IL-1Ra-particles inhibited NF-κB activation to the same levels as an equal amount of soluble IL-1Ra, indicating that the tethered protein retains high bioactivity.

3.7. Effect of IL-1Ra-particles on in vivo protein retention time

We have previously demonstrated the use of near-IR dyes to track and quantify protein retention or release *in vivo* [43,44]. These dyes allow for the non-invasive, repeated imaging of animals without the expense and hazards of radiolabelling. We labeled IL-1Ra with a near-IR dye to track *in vivo* retention for IL-1Ra-tethered particles and soluble protein. Rats received either 5 μg of soluble IL-1Ra or the equivalent amount of IL-1Ra-particles in the stifle joint via intra-articular injection. Rats that received IL-1Ra-particles showed significant fluorescent signal for up to 14 days, while those receiving soluble protein exhibited rapid loss of fluorescent signal (Fig. 5A). Rats treated with IL-1Ra-particles retained 20% signal even at day 10, whereas the soluble IL-1Ra had less than 20% retention at day 3. The IL-1Ra-particles exhibited a significantly longer half-life in the joint compared to the soluble protein (3.01 ± 0.09 days for IL-1Ra-Particles vs. 0.96 ± 0.08 days for soluble IL-1Ra, $p < 0.0001$) (Fig. 5B). We further confirmed retention and distribution of IL-1Ra-tethered nanoparticles in stifle joints using confocal microscopy. Injected Dylight-IR650-tagged IL-1Ra nanoparticles were retained in the joint tissues at large numbers compared to those animals that received soluble Dylight-IR650-tagged IL-1Ra protein (Fig. 6). Nanoparticles were thoroughly distributed throughout intra-articular space and cartilage, while soluble protein was rapidly lost from the knee joints. These results demonstrate that delivery of IL-1Ra via tethering onto nanoparticles significantly enhances *in vivo* protein retention and distribution compared to the soluble protein.

3.8. Structural and phenotypic morphology of the treated rat stifle joint

We have developed a technique to quantify microstructural changes in the articular cartilage using contrast enhanced μCT known as equilibrium partitioning of an ionic contrast agent via μCT (EPIC-μCT) [38]. Monosodium iodoacetate (MIA) induces an arthritic phenotype and was used as a positive control for cartilage degeneration. Rats treated with 1 μg MIA demonstrated significant degeneration of articular cartilage in the medial and lateral plateau, compared to control stifle joints (Fig. 7). On the other hand, rat joints treated with IL-1Ra nanoparticles or the soluble protein did not exhibit detectable changes in cartilage microstructure (Fig. 7).

The stifle joints were also stained histologically to evaluate the effects of the particles on cartilage morphology. No gross differences were observed between joints receiving IL-1Ra-tethered particles and controls (Fig. 8). Histological staining showed dense,

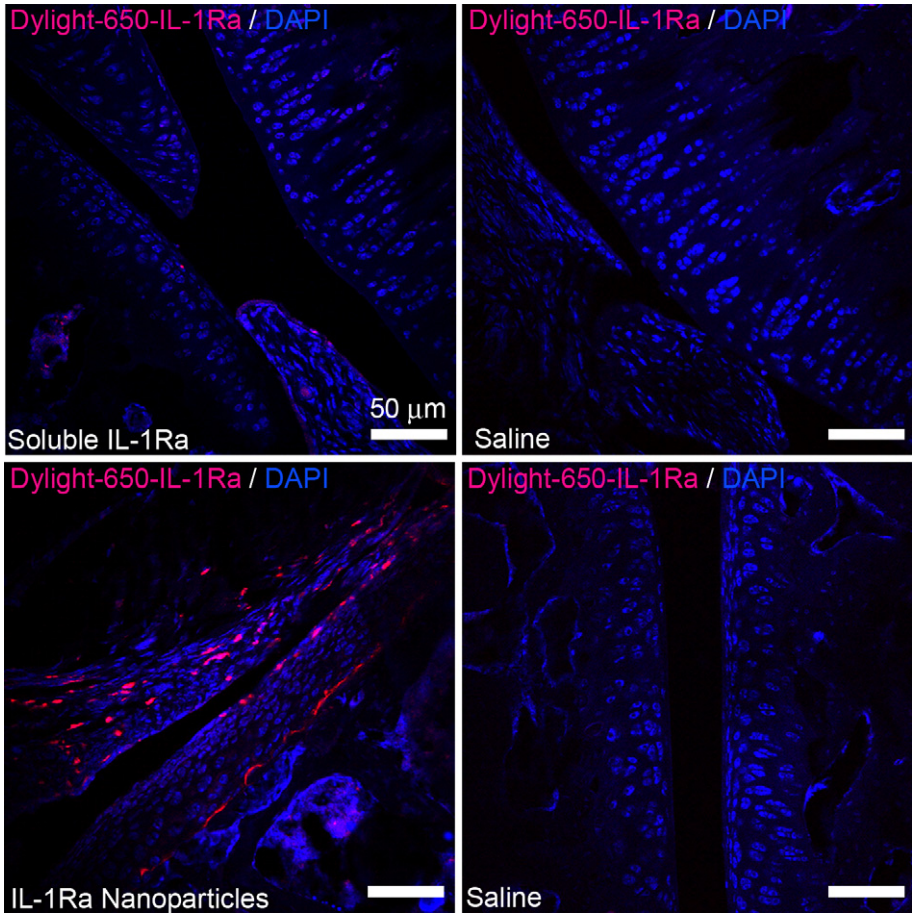

Fig. 6. IL-1Ra-tethered particles are distributed throughout the intra-articular joint space. IL-1Ra was tagged with a Dylight-IR-650 dye prior to tethering IL-1Ra to particles. Tagged IL-1Ra-tethered particles or soluble IL-1Ra was injected into the right stifle joint of 8–10 wk old rats while the left stifle joints received saline. Cryosectioned samples were counterstained with DAPI to localize dye tagged protein. Scale bar = 50 μm.

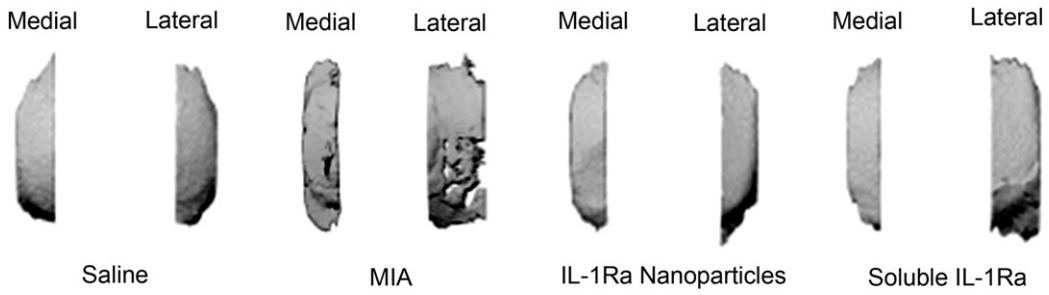

Fig. 7. EPIC-μCT reconstructions of the tibial plateau region cartilage in rats. Representative reconstructions of cartilage from EPIC-μCT analysis. Visual comparisons confirm that there were no gross differences between cartilage receiving IL-1Ra nanoparticles versus soluble IL-1Ra or saline-treated. Rat joints treated with MIA indicated severe cartilage degeneration. Medial side, left; lateral side, right.

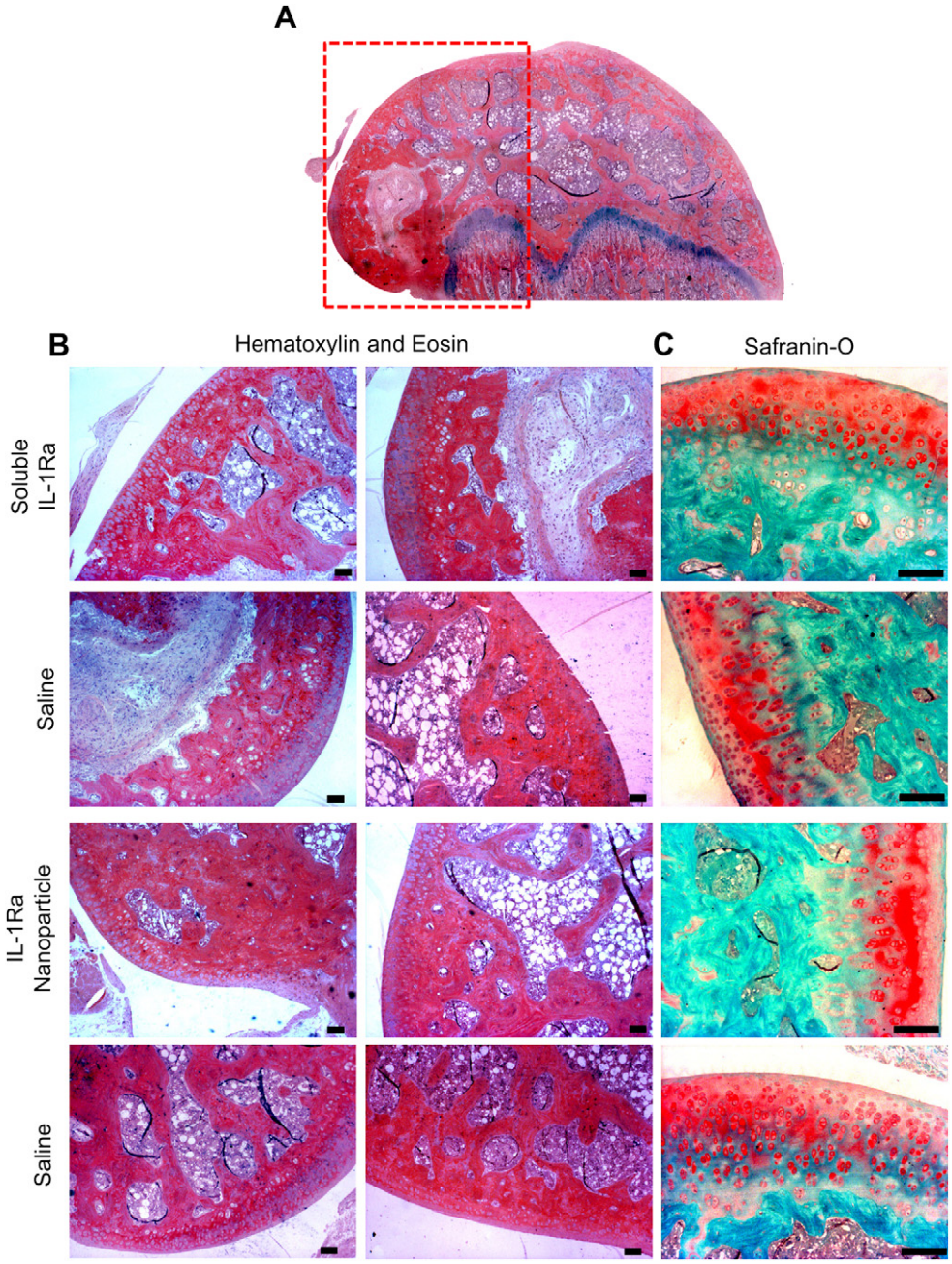

Fig. 8. Histological sections indicating no alterations in cartilage structure and morphology in rats treated with IL-1Ra nanoparticles vs. soluble IL-1Ra or PBS (contralateral). A) Longitudinal section of distal femur indicating the region of interest (red box). All samples were either stained with **B)** hematoxylin and eosin staining, or C) sGAG-staining Safranin-O (scale bar = 100 μm). (For interpretation of the references to color in this figure legend, the reader is referred to the web version of this article.)

uniform distribution of sulfated glycosaminoglycans. Collectively, these results indicate that the IL-1Ra-tethered particles have no gross negative effects on cartilage.

4. Discussion

Intra-articular drug delivery is the most direct route for administering drugs and proteins for arthritis and other joint disorders and conditions. Localized delivery can avoid problems such as systemic toxicity, biological degradation, and biodistribution issues, and can also reduce the total amount of drug used in each treatment. The synovial membrane surrounding the intra-articular joint space creates a compartment that can retain biomolecules larger than 100 kDa [16]. However, most small molecule drugs and proteins are under this cut-off value and are thus cleared quickly from the joint space.

We synthesized an amphiphilic block copolymer that forms self-assembled nanoparticles and allows protein to be tethered to its surface post-nanoparticle formation. Compared to solid polymeric particles, such as PLGA, our nanoparticles provide a hydrophilic environment for presenting an anti-inflammatory protein, IL-1Ra. This hydrophilic environment is expected to maintain protein structure and bioactivity compared to hydrophobic surfaces. Additionally, most current polymer particles do not incorporate a protein tethering moiety on the surface and would require re-engineering the material to add surface-bound targeting ligands [45]. Furthermore, reaction of pNP tethering moiety can be confirmed by release of this group. The pNP tethering moiety is stable at neutral to slightly acidic pH and has a relatively slow decay rate (around 2 h) compared to unstable intermediates of other protein tethering chemistries such as those formed in conventional EDC/NHS reactions. The stability of the pNP moiety allows for a longer reaction time and can increase the efficiency of reaction. These particles are non-cytotoxic up to a concentration of 1 mg/mL in cell culture, which is equivalent to the cytotoxicity of other particles [46,47]. Although the present study focused on 300 nm-diameter particles, we expect that this polymer system can be easily modified to create larger or smaller particles by altering the molecular weight of the block segments. Furthermore, this technology has the potential to incorporate a hydrophobic small molecule drug in the particle core to create a dual therapeutic strategy. The modularity of this copolymer has broad potential to create targeted therapeutic delivery vehicles for a wide range of applications.

The IL-1Ra-tethered polymeric nanoparticles not only retained IL-1Ra bioactivity and its ability to target synoviocytes, but also modulated NF-κB activation after IL-1β stimulation, clearly indicating that IL-1Ra maintains its ability to block the IL-1 signaling pathway. We hypothesize that exploiting IL-1-mediated particle binding to synoviocytes could improve the effectiveness of drug delivery particles for OA by localizing them to inflammatory mediator cells via surface-tethered IL-1Ra. Targeting methods have the potential to increase a particle's residence in the joint. The present work adds to promising targeting strategies, such as phage-panned peptide-targeted nanoparticles [48], hyaluronic acid-coated PLGA particles [49], and chondroitin sulfate-coated gelatin particles [32].

Our results show improved performance to a previously described elastin-like polypeptide-IL-1Ra conjugate "depots" (ELP-IL-1Ra) [30,50]. Although the retention rate of the IL-1Ra-conjugated ELP *in vivo* was similar to that observed for IL-1Ra-tethered particles in the present study, the ELP-IL-1Ra showed a 90% reduction in *in vitro* bioactivity whereas the IL-1Ra-tethered to our nanoparticles retained high bioactivity. By presenting IL-1Ra on the particle surface, we provide cells with easy access to the protein and increase the potency of our particle system. Although effective protein delivery from particles is still a challenge, this work adds to promising strategies, such as the phage-panned peptide-targeted nanoparticles [48], hyaluronic acid-coated PLGA particles [49], and chondroitin sulfate-coated gelatin particles [32].

We demonstrated improved IL-1Ra retention rate by delivering this protein via a nanoparticle compared to direct injection of the soluble protein. Additionally, we showed no deleterious effects in cartilage morphology and structure. These results suggest that these particles may a robust vehicle for intra-articular delivery of therapeutic particles to the joint. Future studies will focus on IL-1Ra delivery to the OA joint and evaluation of therapeutic effectiveness in mitigating cartilage destruction.

5. Conclusions

We synthesized a new block copolymer that assembles into 300 nm-diameter particles with a protein tethering moiety for surface covalent conjugation of IL-1Ra protein. This copolymer particle system efficiently bound IL-1Ra and maintained protein bioactivity *in vitro*. The target specificity of these IL-1Ra-tethered nanoparticles was verified by binding of particle-tethered IL-1Ra to cell surface IL-1 receptors. Importantly, IL-1Ra nanoparticles inhibited IL-1-mediated signaling to equivalent levels as soluble IL-1Ra. Finally, we evaluated the ability of nanoparticles to retain IL-1Ra in the rat stifle joint over 14 days. The IL-1Ra-tethered nanoparticles significantly increased the retention time of IL-1Ra in the rat stifle joint over 14 days and maintained cartilage structure and composition.

Acknowledgments

This work was supported by the Arthritis Foundation, the Georgia Tech/Emory Center (GTEC) for the Engineering of Living Tissues, and the Atlanta Clinical and Translational Science Institute (ACTSI). It was also supported in part by PHS Grant UL1 RR025008 from the Clinical and Translational Science Award program and a National Science Foundation Graduate Fellowship to R.E.W. The authors acknowledge Kellie Templeman for technical support, and Dr. Nick Willett, Tanushree Thote, and Prof. Robert E. Guldberg for training of intra-articular delivery and helpful discussions, and Dr. Angela Lin for technical assistance with EPIC-μCT analyses. We also thank Dr. van de Loo for providing the NF-κB-luciferase NIH 3T3 cells.

References

[1] CDC. Osteoarthritis. Available from: http://www.cdc.gov/arthritis/basics/osteoarthritis.htm; 2011.
[2] Helmick CG, Felson DT, Lawrence RC, Gabriel S, Hirsch R, Kwoh CK, et al. Estimates of the prevalence of arthritis and other rheumatic conditions in the United States. Part I. Arthritis Rheum 2008;58:15–25.
[3] Peyron JG. Epidemiologic and etiologic approach of osteoarthritis. Semin Arthritis Rheum 1979;8:288–306.
[4] Hellio Le Graverand-Gastineau MP. OA clinical trials: current targets and trials for OA. Choosing molecular targets: what have we learned and where we are headed? Osteoarthritis Cartilage 2009;17:1393–401.
[5] Pelletier JP, Martel-Pelletier J, Abramson SB. Osteoarthritis, an inflammatory disease: potential implication for the selection of new therapeutic targets. Arthritis Rheum 2001;44:1237–47.
[6] Zhang W, Moskowitz RW, Nuki G, Abramson S, Altman RD, Arden N, et al. OARSI recommendations for the management of hip and knee osteoarthritis, part II: OARSI evidence-based, expert consensus guidelines. Osteoarthritis Cartilage 2008;16:137–62.
[7] Arner EC, Tortorella MD. Signal transduction through chondrocyte integrin receptors induces matrix metalloproteinase synthesis and synergizes with interleukin-1. Arthritis Rheum 1995;38:1304–14.
[8] Blom AB, van der Kraan PM, van den Berg WB. Cytokine targeting in osteoarthritis. Curr Drug Targets 2007;8:283–92.

[9] Haynes MK, Hume EL, Smith JB. Phenotypic characterization of inflammatory cells from osteoarthritic synovium and synovial fluids. Clin Immunol 2002; 105:315–25.
[10] Pratta MA, Scherle PA, Yang G, Liu RQ, Newton RC. Induction of aggrecanase 1 (ADAM-TS4) by interleukin-1 occurs through activation of constitutively produced protein. Arthritis Rheum 2003;48:119–33.
[11] Chevalier X, Goupille P, Beaulieu AD, Burch FX, Bensen WG, Conrozier T, et al. Intraarticular injection of anakinra in osteoarthritis of the knee: a multicenter, randomized, double-blind, placebo-controlled study. Arthritis Rheum 2009; 61:344–52.
[12] Evans CH, Robbins PD, Ghivizzani SC, Wasko MC, Tomaino MM, Kang R, et al. Gene transfer to human joints: progress toward a gene therapy of arthritis. Proc Natl Acad Sci U S A 2005;102:8698–703.
[13] Frisbie DD, Ghivizzani SC, Robbins PD, Evans CH, McIlwraith CW. Treatment of experimental equine osteoarthritis by in vivo delivery of the equine interleukin-1 receptor antagonist gene. Gene Ther 2002;9:12–20.
[14] Joosten LA, Helsen MM, van de Loo FA, van den Berg WB. Anticytokine treatment of established type II collagen-induced arthritis in DBA/1 mice. A comparative study using anti-TNF alpha, anti-IL-1 alpha/beta, and IL-1Ra. Arthritis Rheum 1996;39:797–809.
[15] Fernandes J, Tardif G, Martel-Pelletier J, Lascau-Coman V, Dupuis M, Moldovan F, et al. In vivo transfer of interleukin-1 receptor antagonist gene in osteoarthritic rabbit knee joints: prevention of osteoarthritis progression. Am J Pathol 1999;154:1159–69.
[16] Perman V. Clinical biochemistry of domestic animals. 3rd ed. Academic Press; 1980.
[17] Wang HJ, Yu CL, Kishi H, Motoki K, Mao ZB, Muraguchi A. Suppression of experimental osteoarthritis by adenovirus-mediated double gene transfer. Chin Med J (Engl) 2006;119:1365–73.
[18] Bias P, Labrenz R, Rose P. Sustained-release dexamethasone palmitate—-pharmacokinetics and efficacy in patients with activated inflammatory osteoarthritis of the knee. Clin Drug Investig 2001;21:429–36.
[19] Horisawa E, Hirota T, Kawazoe S, Yamada J, Yamamoto H, Takeuchi H, et al. Prolonged anti-inflammatory action of DL-lactide/glycolide copolymer nanospheres containing betamethasone sodium phosphate for an intra-articular delivery system in antigen-induced arthritic rabbit. Pharm Res 2002;19: 403–10.
[20] Larsen C, Ostergaard J, Larsen SW, Jensen H, Jacobsen S, Lindegaard C, et al. Intra-articular depot formulation principles: role in the management of postoperative pain and arthritic disorders. J Pharm Sci 2008;97:4622–54.
[21] Johnson BA, Javors MA, Roache JD, Seneviratne C, Bergeson SE, Ait-Daoud N, et al. Can serotonin transporter genotype predict serotonergic function, chronicity, and severity of drinking? Prog Neuropsychopharmacol Biol Psychiatry 2008;32:209–16.
[22] Lee B, Shinohara K, Weinberg V, Gottschalk AR, Pouliot J, Roach 3rd M, et al. Feasibility of high-dose-rate brachytherapy salvage for local prostate cancer recurrence after radiotherapy: the University of California-San Francisco experience. Int J Radiat Oncol Biol Phys 2007;67:1106–12.
[23] Giteau A, Venier-Julienne MC, Aubert-Pouessel A, Benoit JP. How to achieve sustained and complete protein release from PLGA-based microparticles? Int J Pharm 2008;350:14–26.
[24] Lasic DD, Papahadjopoulos D. Medical applications of liposomes. Elsevier; 1998.
[25] Samad A, Sultana Y, Aqil M. Liposomal drug delivery systems: an update review. Curr Drug Deliv 2007;4:297–305.
[26] Gaertner HF, Offord RE. Site-specific attachment of functionalized poly(-ethylene glycol) to the amino terminus of proteins. Bioconjug Chem 1996;7: 38–44.
[27] Gao W, Liu W, Christensen T, Zalutsky MR, Chilkoti A. In situ growth of a PEG-like polymer from the C terminus of an intein fusion protein improves pharmacokinetics and tumor accumulation. Proc Natl Acad Sci U S A 2010; 107:16432–7.
[28] Yu P, Zhang G, Bi J, Lu X, Wang Y, Su Z. Facile purification of mono-PEGylated interleukin-1 receptor antagonist and its characterization with multi-angle laser light scattering. Process Biochem 2007;42:971–7.
[29] Allen KD, Adams SB, Setton LA. Evaluating intra-articular drug delivery for the treatment of osteoarthritis in a rat model. Tissue Eng Part B Rev 2010;16: 81–92.
[30] Shamji MF, Betre H, Kraus VB, Chen J, Chilkoti A, Pichika R, et al. Development and characterization of a fusion protein between thermally responsive elastin-like polypeptide and interleukin-1 receptor antagonist: sustained release of a local antiinflammatory therapeutic. Arthritis Rheum 2007;56: 3650–61.
[31] Bezemer JM, Radersma R, Grijpma DW, Dijkstra PJ, van Blitterswijk CA, Feijen J. Microspheres for protein delivery prepared from amphiphilic multiblock copolymers. 2. Modulation of release rate. J Control Release 2000;67: 249–60.
[32] Brown KE, Leong K, Huang CH, Dalal R, Green GD, Haimes HB, et al. Gelatin/chondroitin 6-sulfate microspheres for the delivery of therapeutic proteins to the joint. Arthritis Rheum 1998;41:2185–95.
[33] Whitaker MJ, Hao J, Davies OR, Serhatkulu G, Stolnik-Trenkic S, Howdle SM, et al. The production of protein-loaded microparticles by supercritical fluid enhanced mixing and spraying. J Control Release 2005;101:85–92.
[34] Wen ZQ, Cao X, Vance A. Conformation and side chains environments of recombinant human interleukin-1 receptor antagonist (rh-IL-1ra) probed by raman, raman optical activity, and UV-resonance Raman spectroscopy. J Pharm Sci 2008;97:2228–41.
[35] Georgescu HI, Mendelow D, Evans CH. HIG-82: an established cell line from rabbit periarticular soft tissue, which retains the “activatable” phenotype. In Vitro Cell Dev Biol 1988;24:1015–22.
[36] Kurz B, Steinhagen J, Schunke M. Articular chondrocytes and synoviocytes in a co-culture system: influence on reactive oxygen species-induced cytotoxicity and lipid peroxidation. Cell Tissue Res 1999;296:555–63.
[37] Smeets RL, Joosten LA, Arntz OJ, Bennink MB, Takahashi N, Carlsen H, et al. Soluble interleukin-1 receptor accessory protein ameliorates collagen-induced arthritis by a different mode of action from that of interleukin-1 receptor antagonist. Arthritis Rheum 2005;52:2202–11.
[38] Palmer AW, Guldberg RE, Levenston ME. Analysis of cartilage matrix fixed charge density and three-dimensional morphology via contrast-enhanced microcomputed tomography. Proc Natl Acad Sci U S A 2006;103:19255–60.
[39] Piscaer TM, van Osch GJ, Verhaar JA, Weinans H. Imaging of experimental osteoarthritis in small animal models. Biorheology 2008;45:355–64.
[40] Xie L, Lin AS, Guldberg RE, Levenston ME. Nondestructive assessment of sGAG content and distribution in normal and degraded rat articular cartilage via EPIC-microCT. Osteoarthritis Cartilage 2010;18:65–72.
[41] Stenzel MH. RAFT polymerization: an avenue to functional polymeric micelles for drug delivery. Chem Commun (Camb) 2008:3486–503.
[42] Kracht M, Weber A, Wasiliew P. Interleukin 1 (IL-1) pathway. science signaling. Washington, D.C: AAAS; 2010. p. The canonical IL-1 signaling pathway, as compiled by Science Signaling.
[43] Boerckel JD, Kolambkar YM, Dupont KM, Uhrig BA, Phelps EA, Stevens HY, et al. Effects of protein dose and delivery system on BMP-mediated bone regeneration. Biomaterials 2011;32:5241–51.
[44] Phelps EA, Landazuri N, Thule PM, Taylor WR, Garcia AJ. Bioartificial matrices for therapeutic vascularization. Proc Natl Acad Sci U S A 2010;107:3323–8.
[45] Singh A, Nie H, Ghosn B, Qin H, Kwak LW, Roy K. Efficient modulation of T-cell response by dual-mode, single-carrier delivery of cytokine-targeted siRNA and DNA vaccine to antigen-presenting cells. Mol Ther 2008;16:2011–21.
[46] Fischer D, Bieber T, Li Y, Elsasser HP, Kissel T. A novel non-viral vector for DNA delivery based on low molecular weight, branched polyethylenimine: effect of molecular weight on transfection efficiency and cytotoxicity. Pharm Res 1999; 16:1273–9.
[47] Fischer D, Li Y, Ahlemeyer B, Krieglstein J, Kissel T. In vitro cytotoxicity testing of polycations: influence of polymer structure on cell viability and hemolysis. Biomaterials 2003;24:1121–31.
[48] Rothenfluh DA, Bermudez H, O'Neil CP, Hubbell JA. Biofunctional polymer nanoparticles for intra-articular targeting and retention in cartilage. Nat Mater 2008;7:248–54.
[49] Zille H, Paquet J, Henrionnet C, Scala-Bertola J, Leonard M, Six JL, et al. Evaluation of intra-articular delivery of hyaluronic acid functionalized biopolymeric nanoparticles in healthy rat knees. Biomed Mater Eng 2010;20: 235–42.
[50] Betre H, Liu W, Zalutsky MR, Chilkoti A, Kraus VB, Setton LA. A thermally responsive biopolymer for intra-articular drug delivery. J Control Release 2006;115:175–82.